ACS APPLIED MATERIALS & INTERFACES

Research Article

www.acsami.org

Electrochromic Properties of Inkjet Printed Vanadium Oxide Gel on Flexible Polyethylene Terephthalate/Indium Tin Oxide Electrodes

Cláudia Costa,[†,‡] Carlos Pinheiro,[§] Inês Henriques,[§] and César A. T. Laia*[,‡]

[†]YDreams, Madan Parque—Sul, 2825-149 Caparica, Portugal

[‡]Requimte, Departamento de Química, Faculdade de Ciências e Tecnologia, Universidade Nova de Lisboa, 2829-516 Caparica, Portugal

[§]Ynvisible, Rua Mouzinho de Albuquerque 7, 2070-104 Cartaxo, Portugal

Supporting Information

ABSTRACT: Vanadium oxide gel was synthesized and formulated for the assembly of solid-state electrochromic cells on flexible and transparent electrodes using inkjet printing. FTIR, Raman, and X-ray diffraction spectroscopic measurements showed that the vanadium oxide gel here synthesized consisted of $V_2O_5 \cdot 6H_2O$, microstructures similar to orthorhombic V_2O_5, while Raman spectroscopy also shows the presence of amorphous domains. Atomic force microscopy (AFM) images of the thin films printed using an inkjet shows a ribbonlike structure, which is in accordance with previous results of the vanadium oxide gels in solution. Solid-state electrochromic devices were assembled at room temperature using the inkjet printed films, without any sinterization step. The electrochemical properties of the vanadium oxide gel were characterized by cyclic voltammetry and spectroelectrochemistry by visible/NIR absorption spectroscopy (in both liquid and solid-state). Several redox steps are observed, which gives rise to a variety of color transitions as a function of the applied voltage. The different optical properties of the vanadium oxide gel are assigned to different intercalation steps of Li^+, leading to different crystalline phases of the gel. The final result is a solid-state electrochromic cell showing excellent contrast between the redox states, giving rise to colors such as yellow, green, or blue. Color space analysis was used to characterize the electrochromic transitions, and while absorption spectra showed rather long switching times (up to 100 s), in $L^*a^*b^*$ color space coordinates, the switching time is smaller than 30 s. These electrochromic cells also have an excellent cycling stability showing high reversibility and a cyclability up to more than 30 000 cycles with a degradation of 18%.

KEYWORDS: *inkjet printing, vanadium oxide, electrochromic devices, nanoparticles, electrochromism, sol—gel*

1. INTRODUCTION

Increasing the color palette for electrochromic devices is one of the major technological challenges of the field. Several compounds proved to have excellent electrochromic performances (such as PEDOT, tungsten oxide, and viologens) that enable their use on commercial applications,[1,2] but those compounds are limited to uncolored/blue transitions. In the latest years, considerable breakthroughs were achieved with organic semiconductor polymers, which increased the color palette dramatically,[3,4] but in terms of using inorganic compounds the palette is still rather small.

In the meantime considerable progress was achieved in the area of printed electronics.[5] With printing deposition techniques, the user may design devices using inexpensive materials and exploring the flexibility for achieving different patterns according with the desired application. This enables the creation of electronic devices on substrates such as plastic foils or paper. Inkjet printing plays an important role in this field, allowing the deposition of conducting surfaces and the construction of transistors, light-emitting devices, and electrochromic cells.[6−8] However, inkjet printing requires inks made of particles with sizes small enough so they do not damage the printer nozzles. To this purpose, organic semiconductor polymers are more suitable for such applications unless metal oxides nanoparticles are synthesized and formulated with the technical specifications for inkjet printing.

Recently we demonstrated that tungsten oxide could be synthesized via a sol—gel method in the form of spherical nanoparticles.[9] These electrochromic devices displayed suitable contrast, switching times, and cyclability. In terms of optical properties, the devices switched between uncolored/blue states as expected for tungsten oxide. One interesting question is if other metal oxide particles could be prepared for the same use, having different color transitions and thus increasing the availability of electrochromic inks for printing techniques. Vanadium oxide indeed presents other colors during its switching (gray, blue, green, and yellow),[10−15] but to our knowledge such material was never deposited into flexible

Received: July 3, 2012
Accepted: September 5, 2012
Published: September 5, 2012

electrodes such as polyethylene terephthalate/indium tin oxide (PET/ITO) using inkjet printing.

Vanadium oxide is normally used for antistatic coatings, humidity sensors, or reversible cathodes in lithium batteries.[16] It may also be used in electrochromic devices, but usually it is a secondary electrochrome for counterelectrode purposes, because the reported color contrast is normally poor and its coloration efficiency is rather low.[17,18] Vanadium oxide materials may be synthesized via sol−gel routes, a synthesis studied and developed during the past years, leading to open structures (gels) formed from aqueous precursors that favor the diffusion of small ionic or molecular species.[12,13,15,16,19] Two types of sol−gel synthesis may be found: by acidification of metavanadate aqueous solutions[15] or by adding hydrogen peroxide to V_2O_5 powder.[20,21] In both cases, $V_2O_5{\cdot}nH_2O$ gels are obtained, and they can be processed for applications such as electrochromism.[11−13,15,16,21−27]

Using sol−gel synthesis with hydrogen peroxide, we show that vanadium oxide gel suitable for inkjet printing may be synthesized. An inkjet formulation was developed and deposited on flexible and transparent PET/ITO electrodes in order to construct solid-state electrochromic devices using the same design developed for tungsten oxide devices. We report its electrochromic performance and show that indeed an excellent color contrast may be achieved with reasonable switching times. The colors range obtained goes from yellow to green, blue, or gray depending of the applied voltage. A characterization of the vanadium oxide material is also shown, using techniques such as X-ray diffraction and Raman spectroscopy, to identify the role of its crystalline state, and a discussion of the electrochromic mechanism of these devices is also made.

2. EXPERIMENTAL SECTION

2.1. Reagents. The following reagents were purchased and used without further purification: vanadium(V) oxide (98+%, Aldrich), hydrogen peroxide (30%, Fluka), lithium perchlorate (98%, Aldrich), and acetonitrile (99.97%, Scharlau). The electrolyte layer was prepared from a mixture containing a polyethylene oxide−polypropylene oxide copolymer (PEO-PPO). This copolymer has an average molecular weight of 150 000 D, and the fraction of PPO is 1% of the weight. The copolymer was dissolved in acetonitrile containing $LiClO_4$. The mass percentages were 24% for the copolymer, 12% for $LiClO_4$, and 64% for acetonitrile. PET/ITO electrodes with a surface resistivity of 60 Ω/sq was purchased from Sigma-Aldrich and used as received.

2.2. Vanadium Oxide Nanoparticle Synthesis. A 1.07 g portion of vanadium(V) oxide was added to 40 mL of hydrogen peroxide. An exothermic reaction occurs spontaneously giving rise to a brown−red paste. This brown−red paste was allowed to dry on a hot plate at 100 °C for 2 h. A brown−red powder is therefore obtained. The composition of the powder was studied using an elemental analysis technique performed in an Elemental Analyzer (Thermo Finnigan-CE Instruments, Italy, model Flash EA 1112 CHNS series). A comparison with the commercially available vanadium oxide powder (used in the synthesis) was performed to determine differences in terms of percentage of carbon and hydrogen elements. The commercially available powder is carbon and hydrogen free. For the synthesized powder, 0.05% (w/w) carbon and 1.34% (w/w) hydrogen were found.

2.3. Ink Formulation. The obtained vanadium oxide powder was dispersed in water (2.54 g/dm^3) and filtered at 1 μm, giving a very stable colloidal suspension (characterized by sedimentation techniques, see the Results and Discussion section). The goal was to obtain a dispersion that could be used as inkjet ink; therefore, viscosity, pH, and surface tension were measured.

2.4. Inkjet Printing. Two drop-on-demand piezo (DOD piezo) inkjet printers (an Epson (Stylus Photo R285) desktop inkjet printer and a lab-scale Dimatix materials printer (DMP-2800)) were used to print the vanadium oxide layer of the electrochromic devices. The vanadium oxide ink was printed on the top of the TCO (transparent conductive oxide) of the PET/ITO electrode. The ink was printed using a waveform with an applied voltage of 26 V and a firing drop frequency of 6 kHz. The drops were small (volume equal to 10 pL, around 10 μm of radius) and spherical as required. A 20 μm drop spacing was employed, and 13 passes were done to obtain the final film.

2.5. Device Assembly. The architecture of the devices is similar to that described for tungsten oxide electrochromic devices (see ref 9), where both electrode and counterelectrode are vanadium oxide films deposited by inkjet printing (see Figure S1 on the Supporting Information). This architecture allows the measurement of light absorption between *oxidized* and *reduced* states, since the patterns of the electrode and counterelectrode are different, the monitored area is selected at one electrode, and it is not overlapped with the image printed at the other electrode. The lithium-based polymer electrolyte was spread-coated on top of one of the vanadium oxide layers and allowed to dry for 1 h (460 μm of thickness). The device was closed and sealed.

2.6. Characterization Techniques. *2.6.1. Dispersion Analysis.* Ink sedimentation velocity and nanoparticle size were determined on different dispersions of sol−gel synthesized vanadium oxide nanoparticles, with a Lumisizer dispersion analyzer (LUM-GmbH, Germany). This apparatus allows acquisition of space- and time-resolved extinction profiles over the sample length. Parallel light (I_0) illuminates the entire sample cell and transmitted light (I) is detected by sensors arranged linearly across the sample from top to bottom. Transmission is converted into extinction coefficient and particle concentration is calculated, therefore, allowing the sedimentation velocity to be determined. Centrifugal force is used to accelerate the sedimentation process. The equipment uses an indirect method to determine the nanoparticles size, using the density of the solid and the liquid phases, the liquid's viscosity, and the sedimentation velocity, by applying Stokes Law.

2.6.2. X-ray Diffraction (XRD), Fourier Transform Infrared Spectroscopy (FTIR), and Raman Spectroscopy. XRD measurements were made on a powder X-ray diffractometer for powders, RIGAKU, model MiniFlex II, 30 kV/15 mA, with copper X-ray tubes. Infrared analyses were performed on a Nicolet Nexus spectrophotometer. Spectra were obtained in absorbance mode, with a resolution of 8 cm^{-1} and 64 scans. Spectra are shown here as acquired, without corrections or any further manipulation, except for baseline correction. The sample consisted of vanadium oxide powder grounded with potassium bromide. This powder mixture was then compressed in a mechanical press to form a translucent pellet through which the spectrophotometer infrared light beam passes. Raman spectroscopy was made in a Labram 300 JobinYvon spectrometer equipped with a He/Ne laser of 17 mW, operating at 632.8 nm and using the vanadium oxide powder.

2.6.3. Differential Scanning Calorimetry (DSC) and Thermogravimetry Analysis (TGA). DSC was performed on the vanadium oxide nanoparticles powder with a calorimeter (Setaram, France) model DSC 131. Temperatures range between −150 and +550 °C. Heating and cooling speeds may be between 0.01 and 99.99 °C/min. The signal of heat flow was between −100 and +100 mW, with a resolution of ±0.2 μW. TGA was performed with a Netzsch STA 409 PC Luxx. The scan temperature was between 40 and 950 °C, and the scan rate was 10 °C/min.

2.6.4. Surface Tension and Viscosity Measurements. Ink surface tension was measured with a KSV Instruments Sigma 70 (Monroe, CT). The DuNoüy ring method was used (R = 9.545 mm, r = 0.185 mm, and l = 119.9 mm), and the surface tension obtained value was corrected following the Zuidema−Waters method. The standard glass beaker had a 66 mm diameter and 110 mL maximum volume. The sample volume used was 80−100 mL. Five measurements were conducted for each sample. Ink viscosity measurements were made with a Brookfield LVT viscometer. Twenty milliliter samples were used to measure three viscosity values at three different velocities: 30,

12, and 6 rpm. A special cylinder (1−100 cP) for low viscosities was used. Density was measured with a 25 mL pycnometer.

These physical characteristics of the fluid are important to achieve an optimum performance of the printing, but they are not limitative. It is possible to print fluids even if the values of surface tension, density, viscosity, and pH are out of the optimal ranges, but the reliability and drop formation may be compromised.

2.6.5. Electrochemical Measurements. Electrochemical measurements on vanadium oxide inkjet printed films were performed in a conventional three-electrode cell. The vanadium oxide film deposited on an PET/ITO electrode was the working electrode, a platinum wire was used as the counterelectrode, a saturated calomel electrode (SCE) was the reference electrode, and the supporting electrolyte was acetonitrile with lithium perchlorate salt (0.1 M). For the solid-state electrochromic device, a two-electrode cell configuration was used. The working electrode and the counterelectrode were both a layer of vanadium oxide film printed on the TCO, with a polymer electrolyte sandwiched between them. The equipment used was a potentiostat/galvanostat Model 20 Autolab from Eco Chemie BV (Utrecht, The Netherlands). The collection of data was controlled by GPES version 4.9 Eco Chemie BV software. No IR compensation was used.

2.6.6. Spectroelectrochemical Measurements. In situ UV/vis absorbance spectra and chronoabsorptometry measurements of the vanadium oxide devices were performed using a UV−vis−NIR spectrophotometer Varian Cary 5000 (spectral range from 220 to 2600 nm). The devices were potentiostatic or potentiodynamically controlled with a potentiostat/galvanostat Model 20 Autolab as described in section 2.6.5. The device was placed in the spectrophotometer compartment perpendicularly to the light beam. The potentiostat/galvanostat applied a square-waveform electric potential (at selected values described below), and the spectrophotometer registered the absorbance at the wavelengths selected for each experiment within the range of the equipment. Stability cycling tests were also performed in the same setup.

2.6.7. Cycling. A camera, a diffuse lamp to control the luminosity (ML series Cold-Cathode Light Panel from Vision Light Tech), and a colorChecker (color pattern) were used to set up a cycling chamber. The electrochromic devices were placed inside the chamber and connected to a function generator. While the function generator applied a determined potential in a square waveform (changing from positive to negative), the camera was setup to record, from time to time, 150 pictures during a calculated period of time, enough to see a complete cycle of the device oxidation and reduction (during several hours, days, or weeks depending on the durability of the device). The pictures were then treated with Matlab software to convert the RGB coordinates obtained from the images into $L^*a^*b^*$ coordinates.

3. RESULTS AND DISCUSSION

3.1. Powder Characterization. XRD, FTIR, and Raman spectroscopy were employed with the aim of characterizing the crystallinity of the synthesized vanadium oxide powder (A). For comparison, the commercially available powder (B, see Experimental Section) was also characterized.

Figure 1 shows the XRD spectra with well-defined peaks for both samples. Nevertheless the crystallinity state is clearly different. Whereas powder B shows diffraction peaks characteristic of orthorhombic V_2O_5 (JCPDS card 41-1426), powder A is typical of a vanadium oxide gel (JCPDS card 40-1296). According to the literature, the vanadium oxide gel with this XRD pattern is an ionic compound with layers of $V_2O_5{\cdot}6H_2O$ and microstructures similar to orthorhombic V_2O_5.[28] It can be described as a nanocomposite build with water molecules entrapped in the V_2O_5 net. Usually this kind of gel presents a ribbonlike structure made with a double layer of VO_5 (like pyramids) facing each other.[15,28] Powder A was sintered at 400 °C, and the same orthorhombic V_2O_5 was obtained (JCPDS card 41-1426).

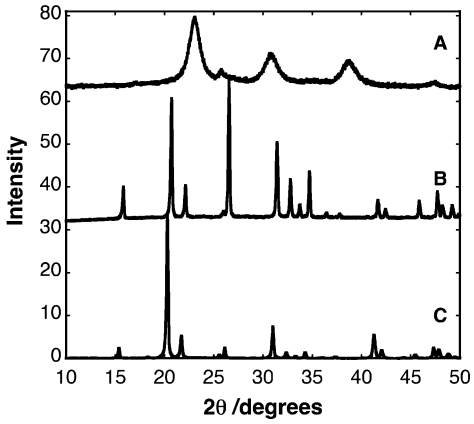

Figure 1. XRD spectra of the synthesized vanadium oxide powder (A, vanadium oxide gel, JCPDS card 40-1296) and commercially available V_2O_5 (B, compatible with orthorhombic V_2O_5 JCPDS card 41-1426). The synthesized powder was sintered at 400 °C, with XRD spectrum shown as well (C, orthorhombic V_2O_5, JCPDS card 41-1426).

FTIR and Raman spectra can provide insights for the presence of an amorphous phase and/or hydration of vanadium oxide. Several revealing features are observed in this set of spectra (see Figure 2). At 3400 and 1615 cm^{-1}, intense absorption IR peaks are observed on powder A. These results were expected since they correspond to vibrational modes of water molecules. For powder B, these peaks are weak. In the region around 1000 cm^{-1}, peaks relative to the V═O terminal oxygen stretching mode are seen in both FTIR and Raman spectra.[29] For powder A, these Raman peaks are split to one weak peak at 1023 cm^{-1} and another strong peak at 892 cm^{-1}. The commercial sample shows a single strong peak at 969 cm^{-1}, in accordance with published results for crystalline V_2O_5.[29] Around 750 cm^{-1} (FTIR), a peak corresponding to a V—O—V asymmetric stretching mode[30] is seen in both powders, but it is shifted to lower wavenumbers in powder A which may indicate the presence of amorphous material in those particles. The Raman spectra show this vibrational mode at 682 cm^{-1} for the commercial sample (characteristic from corner shared oxygen common to 2 pyramids), but it is split into two peaks (706 and 650 cm^{-1}) for the synthesized powder. The appearance of two peaks was already observed earlier for amorphous vanadium oxide, and thus, it can result from the mix of amorphous and crystalline portions in A powder.[31] The same authors also observed two peaks on the 900−1000 cm^{-1} region, concluding that a peak at 932 cm^{-1} is due to V(IV)═O stretching that appears due to oxygen deficiency.[31] If the same reasoning applies to the 892 cm^{-1} peak, that would imply the presence of V(IV) on powder A. At 516 cm^{-1} in FTIR spectra, a V—O—V symmetric stretching mode is found. In Raman spectra, peaks at around 530 cm^{-1} corresponding to V_3O stretching mode from edge-shared oxygen common to three pyramids are found in the two samples.

For lower frequencies, one observes mainly bending modes.[29,31,32] At 483, 405, 283, and 303 cm^{-1} peaks of V—O—V bending mode, V═O bending modes, and V_3O bending mode, respectively, are found in the commercial sample that are equivalent to the peaks found for the synthesized sample at 450 to 200 cm^{-1} but for disordered framework. Finally peaks found above 200 cm^{-1} are typical for lattice modes and it can be notice that those peaks are much less intense in the synthesized sample due to the lack of long-range order.

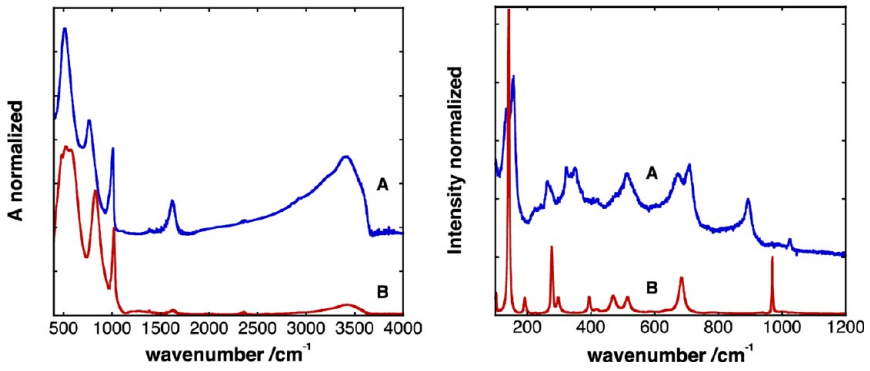

Figure 2. FTIR (left) and Raman (right) spectra of synthesized powder (A) and commercially available V_2O_5 (B).

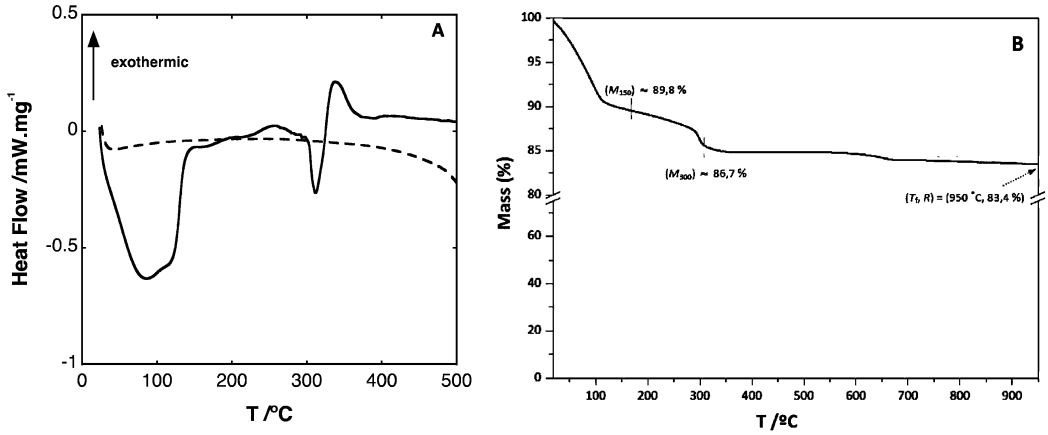

Figure 3. (A) DSC analysis of the vanadium oxide synthesized gel (full line) and of the commercial vanadium oxide (dashed line). Scan rate equal to 10 °C/min. (B) TGA of the vanadium oxide synthesized gel.

Figure 3 shows DSC and TGA of the vanadium oxide powder A and the commercially available V_2O_5 powder B (only DSC in this case). Powder B DSC analysis does not show any transition in the available temperature range (between 25 and 500 °C), as expected since no solvent evaporation or phase transition occurs for this powder within the temperature range. Powder A, however, shows a large endothermic process from room temperature until 140 °C attributed to free water evaporation, confirmed by the loss of mass in this temperature range on the TGA graph (Figure 3B). At 311 °C a sharp second endothermic transition is observed, followed by an exothermic transition at 337 °C. The first process is linked to release of water entrapped within the vanadium oxide structure; see also the TGA graphic in Figure 3B. This process triggers the exothermic transition due to change of the vanadium oxide crystalline state to orthorhombic, as can be seen in Figure 1 (JCPDS card 41-1426, V_2O_5).[14,33] Without the water molecules, the crystalline structure becomes metastable and evolves to the anhydrous crystalline phase.

As described above, sol–gel vanadium oxide normally exists in the form of ribbons.[15] However our synthesis product is the powder of the vanadium oxide gel, which leads to other structures as can be seen on TEM images (Figure 4). Instead, thin sheets of material are synthesized with sizes clearly above 200 nm. AFM images with a lower magnification of the powder (see Supporting Information S2) also shows features in accordance with TEM images: thin sheets are layered, giving a relatively flat appearance. Sahana et al. reported similar results for vanadium oxide gels deposited as thin films deposited by

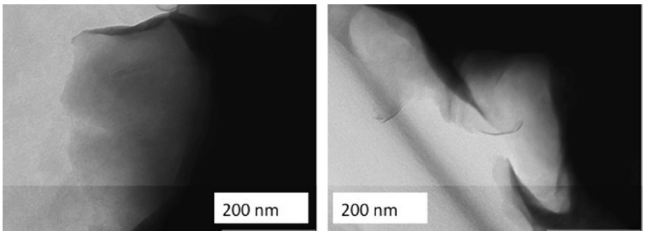

Figure 4. TEM images of the synthesized vanadium oxide powder. These images show the presence of vanadium oxide gel sheet layers (see text).

spin coating followed by baking at 100/350 °C (however on this case, a sinterization step at 450 °C was performed).[14]

The results here presented are therefore in line with those obtained earlier for vanadium oxide gels using the reaction of V_2O_5 as precursor with hydrogen peroxide. As described earlier, the evolution of this mixture evolves initially the formation of water-soluble peroxo species that later decompose to vanadate species. This solution evolves to decavanadic acid that finally polymerizes to $V_2O_5 \cdot nH_2O$ gels.[15,21,25] These pseudocrystalline phases contain both amorphous and crystalline portions, as seen here. 2-Dimensional sheets are observed in the powder, with very large sizes, but as can be seen in the next section, its resuspension in water leads to very stable colloidal particles that can be used in inkjet printing.

3.2. Ink and Inkjet Printing Characterization. The synthesized vanadium oxide powder can be readily suspended on water, producing a formulation with the physical properties

dx.doi.org/10.1021/am301213b | ACS Appl. Mater. Interfaces 2012, 4, 5266–5275

shown on Table 1. For comparison, the optimal values for the use of a given ink formulation on an inkjet printer are also shown.[34] Although optimal conditions are not reached, no defects were observed during the printing process such as satellites, tails, or misdirected nozzles. However because of the high surface tension of the ink, some deposits are observed around the nozzles. This also affects the print quality: instead of having a visually continuous film, as desired, the drops agglomerated to form large domains leading to a printed film with an observable drop pattern. Also, because of the formulation low viscosity, the waveform was calibrated in order to compensate this effect and optimize the printing performance.

Table 1. Values of Surface Tension, Density, Viscosity, and pH for Vanadium Oxide Ink and Optimal Values for the DMP-2800

	ρ (g/cm^3)	η (cP)	surface tension (dyn/cm)	pH
vanadium oxide	1.00	2.2	60	2.5
DMP-2800[34]	≥1	3−12	28−33	3−8

Sedimentation velocity was determined by analytical centrifugation (see the Experimental Section). This type of measurement relies on Stokes law (for particle diffusion under an acceleration field) and Lambert−Beer law (in order to convert optical transmission to particle concentration).

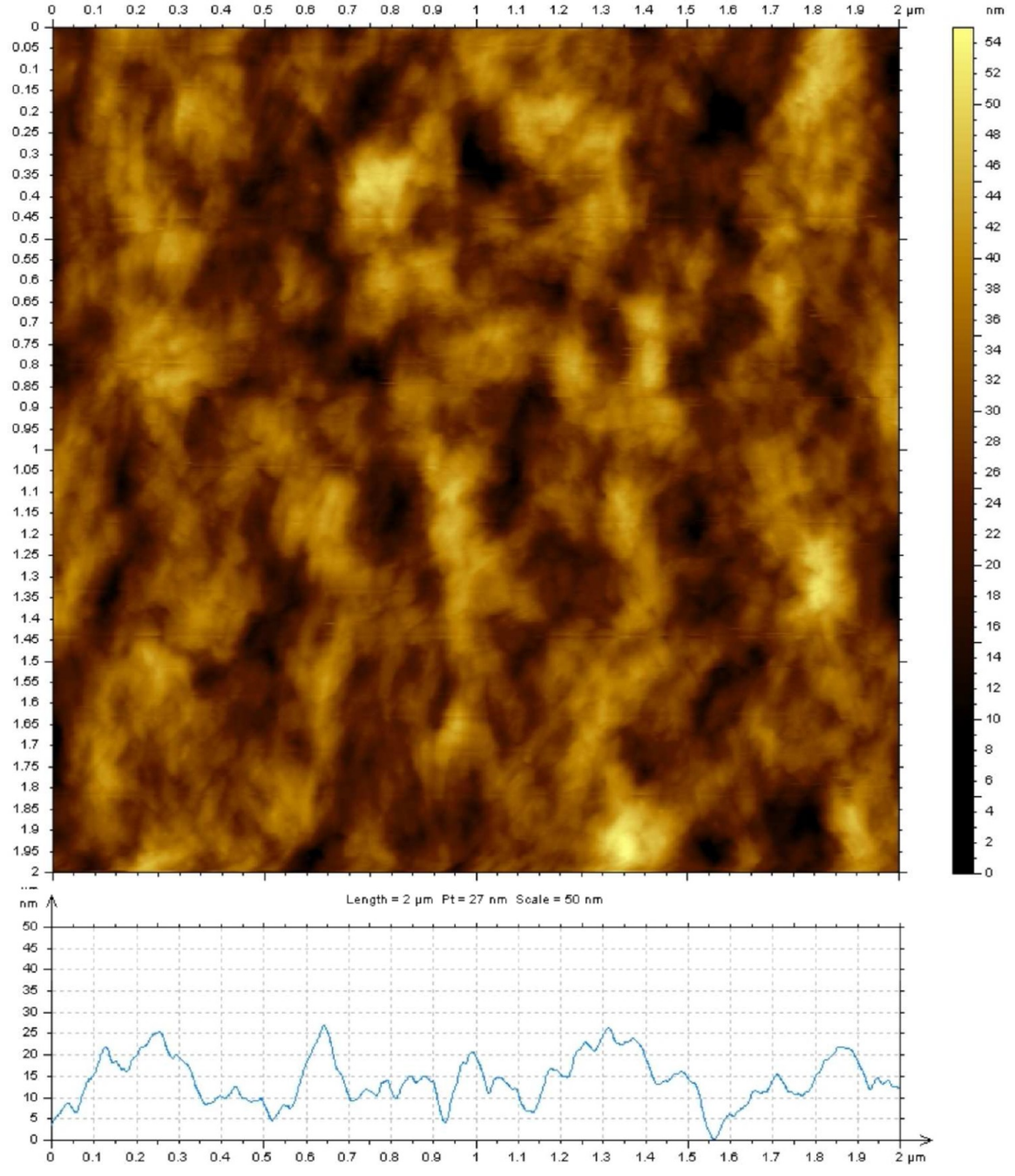

Figure 5. AFM images and rugosity measurements of vanadium oxide gel printed films on PET/ITO substrates.

The profiles of optical transmission vs radial position vs time are obtained at different rotational speeds, and using Lambert–Beer law, it is possible to determine the sedimentation velocity for each angular velocity. In this work, a normalized optical transmission value was chosen in order to avoid meniscus and bottom cell errors.[35]

The sedimentation velocity can be considered a measure of the ink stability. For this case, the experimentally obtained sedimentation velocity (0.018 mm/day) indicates that the ink is very stable and appropriate for this kind of printing method. Due to the small nozzle sizes of common print heads (the nozzle size is typically around 20 μm for a 10 pL drop), inkjet formulations require particles with a size smaller than 1 μm.[36] The nanoparticle average size determined using dynamic light scattering (DLS) measurements was 64 nm of radius, assuming a spherical shape for the particles.

The sedimentation and DLS results clearly are not in accordance with the results obtained for the vanadium oxide powder described above; therefore one may conclude that the particles in solution do not have the same structure observed in the TEM images. Otherwise the ink would not be suitable for inkjet printing since it would damage the nozzles, which is not the case. Atomic force microscopy of the printed film sheds light about this issue (Figure 5). No spherical particles are observed, instead the film has rugosity amplitude of about 30 nm and the pattern of the film looks similar to threads (In Supporting Information S3, the rugosity of the PET/ITO substrate can be seen.). In fact it is known that vanadium oxide gels tend to form ribbons,[15] and that type of structure is compatible with the AFM result. The rugosity of about 30 nm found in AFM measurements could be the average diameter of the ribbons, and the result obtained from DLS (64 nm radius, assuming spherical particles) could reflect the length of these ribbons.

3.3. Electrochemical Characterization. The PET/ITO electrodes coated with vanadium oxide gel by inkjet printing were electrochemically characterized. Figure 6 shows a

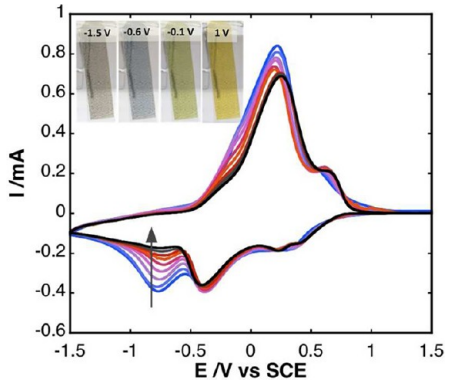

Figure 6. Cyclic voltammetry study for the vanadium oxide synthesized nanoparticles measured at 10 mV/s (10 scans). (inset) Color of the material at different potentials.

characteristic cyclic voltammogram made at 10 mV/s. The wave shows three pairs of oxidation/reduction peaks at −0.23/−0.8, 0.21/−0.4, and 0.64/0.3 V. These peaks give rise to several color transitions: yellow/green, green/blue, and blue/gray, respectively (see insert in Figure 6), which is compatible with results described earlier by other authors.[37] One of those peaks disappears with the number of scans. It is known that the yellow color corresponds to V(V), blue color is V(IV), and violet color is V(II). V(III) has green color,[37] but given the sequence of colors, the green color seen here may arise from the mixture of yellow V(V) and blue V(IV).[1]

The origin of the peak that disappears with the number of scans is not completely clear, but probably it indicates a crystalline phase transition triggered by the oxidation/reduction cycles.[38] The synthesized vanadium oxide gel has at least one crystalline and one amorphous domain, as discussed from XRD and Raman spectra. During electrochemical cycles, Li^+ insertion could change this balance in the first scans, which would explain the disappearance of this peak. On the other hand, some change of morphology with the number of scans may put some sites responsible for such a peak unreachable. Anaissi et al.[38] had similar results with vanadium oxide gel films, in which a so-called "conditioning effect" is described. This effect arises from the intercalation of Li^+ during initial cycles, which in the final steady-state remaining in interlamellar spaces of the vanadium oxide film, and also a more "homogeneous" film is formed. However, while this effect may indeed play a role, the peaks described here are relatively stable. Only one peak disappears after 10 scans. Therefore, the presence of redox sites unreachable after some scans should play a role as well, implying a much more "heterogeneous film" than those described by Anaissi et al.[38]

3.4. Spectroelectrochemistry. The analysis of the color transitions was performed by spectroelectrochemistry in the liquid state (see Figure 7). The absorption spectra on the

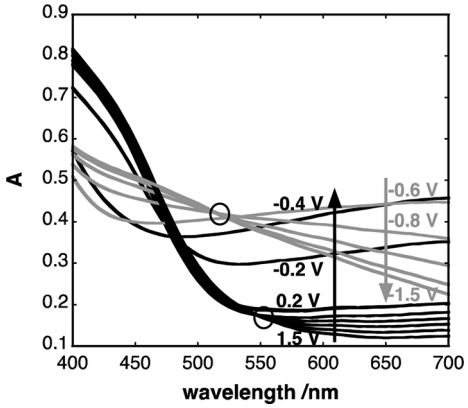

Figure 7. Spectroelectrochemistry in the liquid state for the vanadium oxide inkjet printed film on a PET-ITO electrode. The electrolyte used was acetonitrile with 0.1 M lithium perchlorate. The applied potentials were between 1.5 and −1.5 V (see arrows to see progression of the applied potentials).

visible region is very broad, except for the V(V) state where optical transparency is observed above 600 nm. Several isosbestic points are observed depending of the applied voltage; namely from 0.6 to 1.5 V, from −0.4 to 0.4 V, and from −1.5 to −0.6 V. These ranges are comparable with those observed on the cyclic voltammogram. The physical interpretation of the experimental results should keep in mind that the processes here involved are linked with Li^+ insertion that leads to the formation of $Li_xV_2O_5$ species.[23,39] As discussed in the literature, the partial injection of Li^+ in the interval $0 < x \leq 1$ is responsible for the apparition of three distinct phases, while for $1 < x \leq 2$, Li^+ cannot be entirely deintercalated.[39] This first insertion level ($0 < x \leq 1$) gives rise to different crystalline states of the electrochromic material, reflecting the color

dx.doi.org/10.1021/am301213b | ACS Appl. Mater. Interfaces 2012, 4, 5266–5275

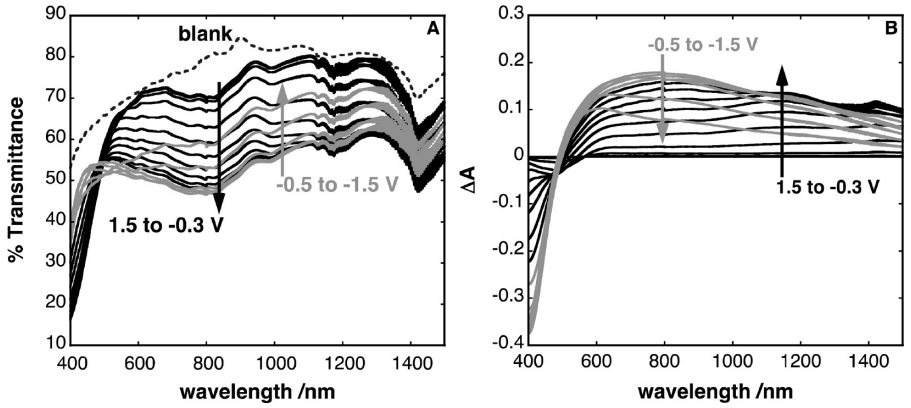

Figure 8. Spectroelectrochemistry in solid state for the vanadium oxide inkjet printed cell on PET-ITO electrodes. (A) Transmittance spectra varying with the applied potential. The dotted line is the device without the electrochromic material (blank). (B) Differential absorption spectra (1.5 V absorption spectrum was used as reference). See arrows to see progression of the applied potentials.

changes observed. The formation of a broad band for higher wavelengths is indicative of the presence of V(IV), which through intervalence-transfer interactions with V(V) explains its appearance.[38] However our results show that even the synthesized powder has a crystalline and amorphous fractions, and therefore, each fraction will have different Li^+ insertion processes.[10,12,14,23,39] In a recent publication with tungsten oxide electrochromic cells, such an effect was observed leading to unambiguous results on spectroelectrochemical experiments.[9] But for vanadium oxide, unfortunately, such an effect was not clearly observed because the NIR region was not measured with the current experimental setup. However this region could be analyzed for the solid-state electrochromic cells.

The optical properties of the vanadium oxide gel films in a solid-state electrochromic cell were characterized by vis−NIR spectroelectrochemistry in the wavelength range of 400−1500 nm and voltage range of −1.5 to 1.5 V. The solid-state electrochromic cell contains all components of the device, including the TCO and electrolyte layers, each one contributing for the light absorption. Figure 8A shows the changes of the transmittance spectra by applying voltage to the device. At all wavelengths, the applied voltage induces optical changes. As in the liquid state, the more transparent state is reached when 1.5 V is applied, where significant light absorption exists only for wavelengths lower than 600 nm (and therefore explaining its yellow color corresponding to V(V)). As the material is reduced, light absorption gradually becomes significant at all wavelengths.

Figure 8B shows the differential absorption spectra using the most transparent state as reference (1.5 V). For applied voltages lower than 1.5 V, gradually a large absorption band appears raging from about 600 nm to wavelengths above 1500 nm. This broad band gives information in the NIR region not shown for liquid-state. Its band peak consistently shifts to lower wavelengths (or higher energies) when the applied voltage is more negative. However no isosbestic point is observed in the NIR region: instead the observed change of the absorption is gradually shifting. This result points to a gradual Li^+ insertion on the optical layer, changing the relative fraction of V(IV) and V(V) species and probably the crystalline state of the vanadium oxide gel as well, which also depends of the number of scans but with changes much less evident than in the liquid cell (see Figure S4 in the Supporting Information). The maximum electrochromic effect is seen at −0.9 V, where the blue color is more intense (see color space analysis below). Such processes are reflected on the transient measurement in Figure 9. The

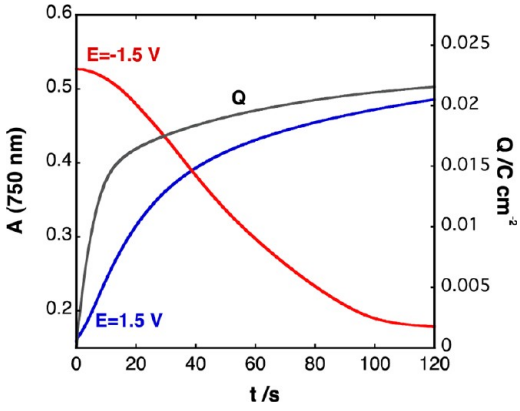

Figure 9. Response time study at 1.5 and −1.5 V measured at 750 nm. The red line is the absorption change during the oxidation process, the blue line is that during the reduction process, and black line is the charge consumption for the oxidation process.

oxidation leads to absorption increase at 750 nm on a time-scale of about 30 s with two distinct regimes, while the reduction is slightly slower with no distinct regime. These results point out a rather heterogeneous vanadium oxide layer, with different crystalline phases (probably those observed in the XRD experiments).

3.5. Device Performance: Lab Color Space, Cycling, and Coloration Efficiency. The performance of the solid-state electrochromic cell described above was evaluated by measuring the color coordinates during the switching, its degradation with the number of electrochemical cycles and the coloration efficiency. Figure 10 shows the CIE Lab color coordinates calculated for both liquid-state and solid-state measurements as a function of the applied voltage. This calculation was done from the optical absorption spectra in the visible range (400−700 nm), using the Standard Iluminant CIE D65 and calculating the trichromatic individual coordinates X, Y, and Z:[40]

$$X = \sum E_i x_i T_i \quad (1)$$

where E_i is the coefficient of the Standard Iluminant CIE, x_i is the coefficient of the tristimulus value, and T_i is the optical

dx.doi.org/10.1021/am301213b | ACS Appl. Mater. Interfaces 2012, 4, 5266−5275

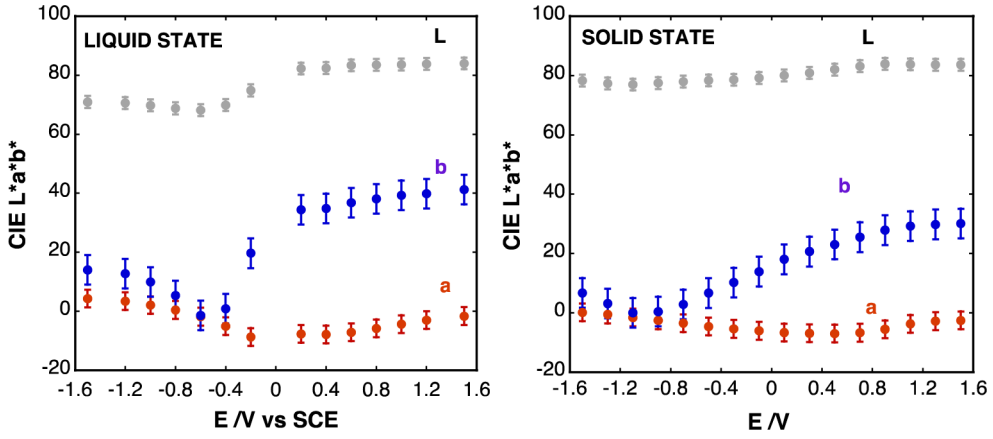

Figure 10. CIE Lab color coordinates calculated for liquid-state (left) and solid-state (right) measurements as a function of the applied voltage.

transmittance, all for a given wavelength λ_i (the same type of calculation is done for Y and Z).

X, Y, and Z values then be converted to $L^*a^*b^*$ color coordinates using the following equations:

$$L^* = 116\left(\frac{Y}{Y_n}\right)^{1/3} - 16 \quad (2)$$

$$a^* = 500\left[\left(\frac{X}{X_n}\right)^{1/3} - \left(\frac{Y}{Y_n}\right)^{1/3}\right] \quad (3)$$

$$b^* = 200\left[\left(\frac{Y}{Y_n}\right)^{1/3} - \left(\frac{Z}{Z_n}\right)^{1/3}\right] \quad (4)$$

where X_n, Y_n, and Z_n is the white color values with the illuminant used. These equations are valid as long the quotients X/X_n, Y/Y_n, and Z/Z_n are greater than 0.008 856 (which is normally the case).

Qualitatively, these results are rather similar to those obtained from absorption spectra since they are interrelated. However, one can clearly see that in terms of optical contrast it is b^* (blue/yellow coordinate) that has more significant changes. A more negative value means a blue perception by the eye, which for the liquid state is reached around −0.5 V (vs SCE) while in the solid-state electrochromic cell (including all parts of the device, namely PET/ITO electrodes and electrolyte layer) it shifts to around −1.1 V. In the second case, between −1.5 and −1.1 V the colors are quite similar.

To calculate the color coordinates during the electrochromic transition of the solid-state cell, a setup with a digital camera under diffuse light inside a room was used (see Experimental Section). Afterward the images were analyzed by calibration with a ColorChecker, in order to calculate L^*, a^*, and b^*. These results were then converted to color contrast values ΔE^* (Figure 11) using the oxidized state as reference (1.5 V), after calculating ΔL^*, Δa^*, and Δb^*:[41]

$$\Delta L^* = |L^*_{ox} - L^*(t)| \quad (5a)$$

$$\Delta a^* = |a^*_{ox} - a^*(t)| \quad (5b)$$

$$\Delta b^* = |b^*_{ox} - b^*(t)| \quad (5c)$$

$$\Delta E^* = \sqrt{(\Delta L^*)^2 + (\Delta a^*)^2 + (\Delta b^*)^2} \quad (5d)$$

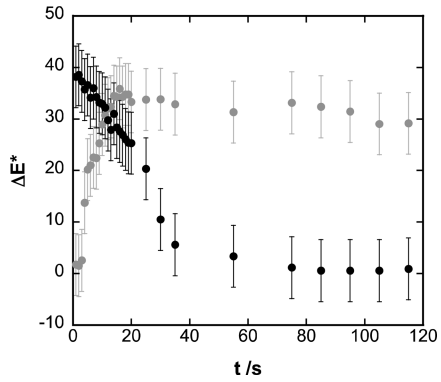

Figure 11. Color contrast values (ΔE^*) for the oxidation (black) and reduction processes (gray).

The results indicate that after 30 s the available device optical contrast is reached, and therefore, this is the practical response time of the device.

The device stability was tested by *on/off* cycling, by alternating between the two states of the device at a given voltage and monitoring the performance at 750 (see Figure 12). For the −1.5/+1.5 V cycles, the color stability can be measured and is very good after 1000 cycles and rather constant. The stability of the device was also monitored using $L^*a^*b^*$ coordinates, as described in the Experimental Section and

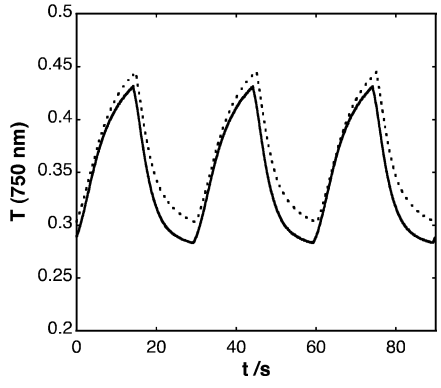

Figure 12. Device stability tested by *on/off* cycling, by alternating between −1.5 and +1.5 V and monitoring the performance at 750 nm. Black line is the device performance when assembled, and the dotted line is the performance after 1000 cycles.

dx.doi.org/10.1021/am301213b | ACS Appl. Mater. Interfaces 2012, 4, 5266−5275

allowing it to perform a long cycling measurement. The device achieved 30 000 cycles with 18% of degradation (see the Supporting Information).

Table 2 shows more details about the electrochromic performance of the device. The coloration time τ_c and bleaching time τ_b were measured as the time necessary to obtain 95% of the total optical transmittance contrast at 750 nm from data similar to those shown on Figure 9, as well as the electric current and the so-called coloration efficiency CE at 750 nm. The total charge Q is equal on either coloration or bleaching steps, which is essential for a good long-term cyclability. Coloration efficiency has typical values for vanadium oxide. The switching times, however, are rather long. Those values were taken from changes of the absorption spectra, and it is not in accordance with the color contrast changes seen on $L^*a^*b^*$ color coordinates (about 30 s). We think that this result shows that for materials where color transitions do not involve a transparent state, a good color switching time may be reached before the system is stabilized in terms of optical transmittance. Color coordinates indeed give faster switching times, in accordance with the user perception. Transmittance switching times shown in Table 2 are useful because they give an insight of the molecular reaction kinetics. So while switching times are clearly slower than for other materials such as tungsten oxide, vanadium oxide gels still may be used in the future in electrochromic devices that require switching times until about 30 s.

Table 2. Electric Current, Transition Time between Colored and Bleached States, Coloration Efficiency, Change in Absorbance and in Transmittance at 750 nm of a Flexible Electrochromic Device Built with the Vanadium Oxide Printed Films on PET/ITO Using Powder A

voltage/V	Q (mC/cm^2)	$\Delta\%T$ (±0.5%)	ΔA (±0.002)	CE (cm^2/C; ±1 cm^2/C)	τ_c (s; ±2 s)	τ_b (s; ±2 s)
0.1	0.70	4.1	0.030	42	230	230
0.3	2.31	12.4	0.095	42	208	196
0.5	4.18	20.4	0.164	40	192	170
0.7	6.45	26.3	0.225	36	186	166
0.9	9.14	33.0	0.295	33	195	150
1.1	11.54	37.1	0.342	30	184	118
1.3	13.05	37.8	0.352	27	139	92
1.5	22.38	39.6	0.398	16	143	103

Until now, few electrochromic devices using inkjet printing as deposition technique for the electrochromic layer were reported.[8,9] The results here shown demonstrate that vanadium oxide may also be deposited by inkjet with excellent color contrast and stability. The coloration efficiencies of the present device are similar to those described earlier using deposition techniques such as pulsed spray pyrolysis[42] (CE = 13 cm^2/C, $\Delta\%T$ around 30%, similar switching times and stability up to 10 000 cycles), chemical bath deposition[43] ($\Delta\%T$ around 20%), sputtering[44] ($\Delta\%T$ around 40%), or sol–gel based depositions such as spin-coating[26] (CE = 20 cm^2/C). To our knowledge, the best performance with vanadium oxide electrochrome was recently achieved by Scherer et al.,[45] where an impressive switching time smaller than 1 s and very high CE were obtained on mesoporous film of vanadium oxide (CE = 3500 cm^2/C, $\Delta\%T$ around 50%, stability up to about 10^2 cycles with 20% degradation). In this case the high porosity of the film greatly enhances Li^+ insertion. Comparing with the literature, the greatest achievement of the results here presented is the possibility to use inexpensive inkjet printing, without annealing, and using flexible PET/ITO electrodes to obtain electrochromic devices with a performance that matches those reported in the literature. Currently the color palette available for electrochromic devices is dramatically expanding due to the use of organic semiconductor polymers.[3,4] This work shows that inorganic metal–oxide nanoparticles also have potentialities and might be used in the near future in commercial applications.

4. FINAL COMMENTS

Vanadium oxide gels powders were synthesized using V_2O_5 and hydrogen peroxide as reagents. An inkjet formulation of this gel is proposed by dispersion in water, which was deposited on the surface of flexible and heat sensitive PET/ITO electrode using inkjet printing. Particles of about 64 nm of radius are found from DLS experiments of the vanadium oxide gel aqueous dispersion and ribbonlike structures may be seen on printed films using AFM. It is demonstrated that such vanadium oxide coatings have electrochromic activity with a good color contrast. Spectroelectrochemical measurements evidenced three isosbestic points attributed to the transition between only two different oxidation states (V(V) and V(IV)) that happens in three different phases depending on the applied potential, changing the structure of the crystalline parts, and the color observed. The electrochromic cells response time is much faster when calculated using contrast color through CIE Lab color space and slower when calculated using the absorption spectra, pointing out the necessity of crosschecking the optical performance using both approaches when the samples do not have an uncolored state. The large NIR electrochromism is similar to that observed with tungsten oxide, due to intervalence-transfer interactions; therefore, these systems would have applications on devices where NIR transmittance should be controlled (such as intelligent windows).

■ ASSOCIATED CONTENT

Supporting Information

Design of the solid-state electrochromic cells, AFM images of the synthesized powder, rugosity of PET/ITO substrates, cyclic voltammetry of a solid-state electrochromic cell, and degradation upon cycling. This material is available free of charge via the Internet at http://pubs.acs.org.

■ AUTHOR INFORMATION

Corresponding Author

*Tel.: + 351 212948355. Fax: + 351 212948385. E-mail address: catl@fct.unl.pt.

Notes

The authors declare no competing financial interest.

■ ACKNOWLEDGMENTS

This work has been supported by Fundação para a Ciência e a Tecnologia through grant no. PEst-C/EQB/LA0006/2011. Financial support from Fundação para a Ciência e a Tecnologia (FCT-MCTES; project PTDC/CTM-NAN/120658/2010), QREN-SI I&DT Mobilizadores–Project Invisible Network (no. 13857), and QREN-SI I&DT Co-Promoção–Project YMagazines (no. 13745) is acknowledged. C.C. acknowledges FCT-MCTES and YDreams for Ph.D. grants (SFRH/BDE/33291/2008). The Restoration and Conservation Department

at Faculdade de Ciências e Tecnologia is acknowledged for the FTIR and Raman Spectroscopy equipment used in the characterization measurements. CENTI, Centre for Nanotechnology and Smart Materials, is acknowledged for the AFM measurements.

REFERENCES

(1) Monk, P. M. S.; Mortimer, R. J.; Rosseinsky, D. R. In *Electrochromism and Electrochromic Devices*; Cambridge University Press: Cambridge, United Kingdom, 2007.
(2) Granqvist, C. G. In *Handbook Of Inorganic Electrochromic Materials*, Elsevier: The Netherlands, 2002.
(3) Beaujuge, P. M.; Reynolds, J. R. *Chem. Rev.* **2010**, *110*, 268−320.
(4) Amb, C. M.; Dyer, A. L.; Reynolds, J. R. *Chem. Mater.* **2011**, *23*, 397−415.
(5) Nathan, A.; Chalamala, B. R. P. *IEEE* **2005**, *93*, 1235−1238.
(6) Yan, H.; Chen, Z.; Zheng, Y.; Newman, C.; Quinn, J. R.; Dotz, F.; Kastler, M.; Facchetti, A. *Nature* **2009**, *457*, 679−686.
(7) Bharathan, J.; Yang, Y. *Appl. Phys. Lett.* **1998**, *72*, 2660−2662.
(8) Andersson, P.; Forchheimer, R.; Tehrani, P.; Berggren, M. *Adv. Funct. Mater.* **2007**, *17*, 3074−3082.
(9) Costa, C.; Pinheiro, C.; Henriques, I.; Laia, C. A. T. *ACS Appl. Mater. Interfaces* **2012**, *4*, 1330−1340.
(10) Cogan, S. F; Nguyen, N. M.; Perrotti, S. J.; Rauh, R. H. *J. Appl. Phys.* **1989**, *66*, 1333−1337.
(11) Nagase, K.; Shimizu, Y.; Miura, N.; Yamazoe, N. *Appl. Phys. Lett.* **1992**, *60*, 802−804.
(12) Livage, J. *Solid State Ionics* **1996**, *86*−*88*, 935−942.
(13) Livage, J.; Guzman, G.; Beteille, F.; Davidson, P. *J. Sol*−*Gel Sci. Technol.* **1997**, *8*, 857−865.
(14) Sahana, M. B.; Sudakar, C.; Thapa, C.; Lawes, G.; Naik, V. M.; Baird, R. J.; Auner, G. W.; Naik, R.; Padmanabhan, K. R. *Mater. Sci. Eng., B* **2007**, *143*, 42−50.
(15) Livage, J. *Chem. Mater.* **1991**, *3*, 578−593.
(16) Livage, J.; Beteille, F.; Roux, C.; Chatry, M.; Davidson, P. *Acta Mater.* **1998**, *46*, 743−750.
(17) Rauh, R. D.; Cogan, S. F. *Solid State Ionics* **1988**, *28*−*30*, 1707−14.
(18) Ashrit, P. V.; Girouard, F. E.; Truong, V. V. *Solid State Ionics* **1996**, *89*, 65−73.
(19) Livage, J. *Coordin. Chem. Rev.* **1998**, *178*−*180*, 999−1018.
(20) Düllberg, P. *Z. Phys. Chem.* **1903**, *45*, 129.
(21) Alonso, B.; Livage, J. *J. Solid State Chem.* **1999**, *148*, 16−19.
(22) Hibino, M.; Ugaji, M.; Kishimoto, A.; Kudo, T. *Solid State Ionics* **1995**, *79*, 239−244.
(23) Talledo, A.; Granqvist, C. G. *J. Appl. Phys.* **1995**, *77*, 4655−4666.
(24) Ozer, N. *Thin Solid Films* **1997**, *305*, 80−87.
(25) Vivier, V.; Farcy, J.; Pereira-Ramos, J. P. *Electrochim. Acta* **1998**, *44*, 831−839.
(26) Wang, Z. C.; Chen, J. F.; Hu, X. F. *Thin Solid Films* **2000**, *375*, 238−241.
(27) Sahana, M. B.; Sudakar, C.; Thapa, C.; Lawes, G.; Naik, V. M.; Baird, R. J.; Auner, G. W.; Naik, R.; Padmanabhan, K. R. *Mater. Sci. Eng., B* **2007**, *143*, 42−50.
(28) Lei, S.; Tang, K.; Jin, Y.; Chen, C. *Nanotechnology* **2007**, *18*, 175605.
(29) Baddour-Hadjean, R.; Pereira-Ramos, J. P. *Chem. Rev.* **2010**, *110*, 1278−1319.
(30) Jin, A.; Chen, W.; Zhu, Q.; Yang, Y.; Volkov, V. L.; Zakharova, G. S. *Solid State Ionics* **2008**, *179*, 1256−1262.
(31) Lee, S.; Cheong, H.; Seong, M.; Liu, P.; Tracy, C. E.; Mascarenhas, A.; Pitts, J. R.; Deb, S. K. *J. Appl. Phys.* **2002**, *2*, 1893−1897.
(32) Surca, A.; Orel, B.; Drazic, G.; Pihlar, B. *J. Electrochem. Soc.* **1999**, *146*, 232−242.
(33) Wang, Y.; Shang, H. M.; Chou, T.; Cao, G. Z. *J. Phys. Chem. B* **2005**, *109*, 11361−11366.
(34) *DMP-2800 Materials Printer User Manual*; Dimatix.
(35) Detloff, T.; Sobisch, T.; Lerche, D. *Powder Technol.* **2007**, *174*, 50−55.
(36) Calvert, P. *Chem. Mater.* **2001**, *13*, 3299−3305.
(37) Lee, J. D. *Concise Inorganic chemistry*; Chapman & Hall: England, 1996.
(38) Anaissi, F. J.; Demets, G. J. F.; Toma, H. E. *Electrochem. Commun.* **1999**, *1*, 332−335.
(39) Bay, N. T. B.; Tien, P. M.; Badilescu, S.; Djaoued, Y.; Bader, G.; Girouard, F. E.; Truong, V. V.; Nguyen, L. Q. *J. Appl. Phys.* **1996**, *80*, 7041−7045.
(40) Brotherston, I. D.; Mudigonda, D. S. K.; Osborn, J. M.; Belk, J.; Chen, J.; Loveday, D. C.; Boehme, J. L.; Ferraris, J. P.; Meeker, D. L. *Electrochim. Acta* **1999**, *44*, 2993−3004.
(41) Tehrani, P.; Hennerdal, L. O.; Dyer, A. L.; Reynolds, J. R.; Berggren, M. *J. Mater. Chem.* **2009**, *19*, 1799−1802.
(42) Patil, C. E.; Tarwal, N. L.; Shinde, P. S.; Deshmukh, H. P.; Patil, P. S. *J. Phys. D: Appl. Phys.* **2009**, *42*, 025404.
(43) Najdoski, M.; Koleva, V.; Demiri, S. *Mater. Res. Bull.* **2012**, *47*, 737−743.
(44) Lin, Y. S.; Tsai, C. W. *Surf. Coat. Technol.* **2008**, *202*, 5641−5645.
(45) Scherer, M. R. J.; Cunha, P. M. S.; Scherman, O. A.; Steiner, U. *Adv. Mater.* **2012**, *24*, 1217−1221.